A Molecular Dynamics Study of Methyl Group Rotation in Poly(vinyl methyl ether)

C. Saelee, T. M. Nicholson,* and G. R. Davies

IRC in Polymer Science and Technology, University of Leeds, Leeds LS2 9JT, U.K.

Received July 30, 1999; Revised Manuscript Received January 3, 2000

ABSTRACT: This paper presents a molecular modeling study of the methyl group rotations in poly(vinyl methyl ether) (PVME), which are sufficiently fast to be accessible by molecular dynamics. Simulation cells were produced and validated by a comparison of simulated X-ray scattering data with experimental measurements. The behavior of the methyl groups was analyzed in terms of transitions between three equivalent states both directly in terms of the transition rate and also by fitting a conformational state autocorrelation function. The results compare well with those of neutron scattering data available in the literature. A detailed study of individual group behavior shows that at high temperatures all methyl groups tend to behave in a similar fashion, with each methyl group exhibiting a nonexponential decay of the correlation function, while at lower temperatures individual groups behave differently, each group tending to a single-exponential decay of the correlation function but with a wide range of decay times.

Introduction

We are interested in studying methods whereby sub-T_g motions in polymers may be modeled. Our initial studies were performed on poly(methyl methacrylate) (PMMA)[1] where the motion of the carbonyl methyl groups is sufficiently fast to be accessible by molecular dynamics (MD) techniques, and there were experimental quasi-elastic neutron scattering data[2] available. The motion of the methyl group is assumed to be transitions between three identical states, and the experimental data were analyzed in terms of a stretched exponential, or Kohlraush−Williams−Watts (KWW) function,[3] which accounts for a distribution of transition frequencies between states. The parameters to be fitted in this function are the transition attempt frequency ($1/\tau$), the temperature variation of which leads to a calculation of the activation energy of the process, and the exponent β, which gives a measure of the range of relaxation times present in the motion. This last factor is relatively insensitive to different experimental (or simulation) conditions.

An alternative approach, applied to the methyl group rotation in poly(vinyl methyl ether) (PVME) by Colmenero et al.,[4,5] is to analyze experimental data in terms of a rotation rate distribution model (RRDM), which considers a distribution of transition rates. The mean rate and spread of rates are functions of temperature. The RRDM has been successfully applied to analyze experimental data for methyl group rotations in several polymers, over a wide range of temperatures both in the classical regime and at very low temperatures (∼2 K) in the quantum regime. The RRDM parameters are easily calculated from MD simulations, and so in this paper we describe the modeling of the methyl group rotations in PVME. These are analyzed in terms of both the KWW and RRDM fits and compared to the experimental data.

At low temperatures quantum tunneling through the barrier is the dominant process, but as the temperature is increased, the rate of quantum tunneling decreases[6] while the rate of thermally activated jumping over the barrier increases until this is the dominant process above about 70 K. The motion at 200 K and above, which is considered in this work, can therefore be considered in classical terms.

This work stems from our aims to understand the mechanisms involved in sub-T_g relaxation processes in polymers. Many of these occur over a time scale that is too slow to be accessible by conventional MD techniques, where one is typically restricted to simulation times of below 10^{-8} s. Other methods have thus been explored such as the quasi-static minimization technique[1] where a transition path is explored by systematically altering a chosen coordinate, while minimizing the rest of the structure. Studies, such as those reported here, where MD techniques are accessible allow for a comparison with these other methods.

Simulation Cell Construction and Validation

The simulations were performed on a model system of amorphous PVME constructed using functionality in the InsightII package from MSI.[7] An atactic polymer chain consisting of 180 repeat units was built with a meso-dyad probability of 0.64, corresponding to the experimentally measured value obtained by ^{13}C NMR at the IRC in Polymer Science and Technology at the University of Durham. This chain was then placed into a cubic simulation box with periodic boundary conditions. The method used to place the chain in the box chose a distribution of torsions along the backbone of the polymer corresponding to a temperature of 500 K. This method of cell construction follows an improved version of the Theodoro and Suter method[8] where units are added to a growing chain at Boltzmann-weighted dihedrals incorporating lookahead[9] where the energetics of adding several bonds is tested rather than simply adding single bonds. Initially the cell was built with a low density, and then molecular dynamics (MD) were run at constant pressure to refine the structure (relax any near overlapping of atoms) and to increase the density to its experimental value of 0.9 g cm^{-3}, to yield a simulation cell of side ∼26 Å. A total of five simulation cells were independently constructed.

Cells at lower temperatures were generated from the initial cells by running MD, while reducing the temperature of the simulation in steps from 500 to 200 K.

10.1021/ma991267p CCC: $19.00
Published on Web 02/25/2000

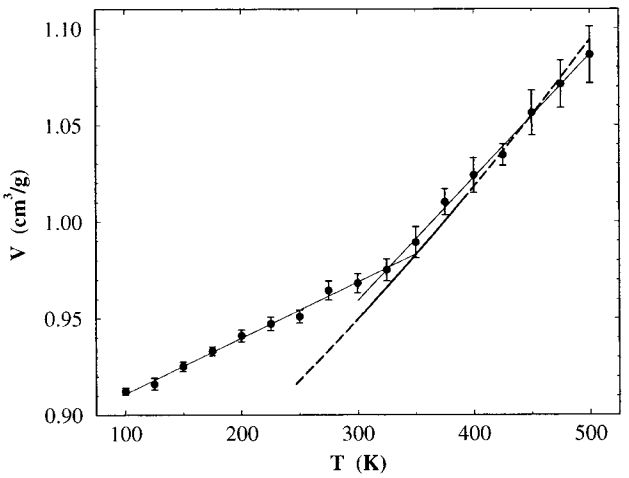

Figure 1. Volume vs temperature obtained during cooling of one simulation cell from 500 to 200 K in 25 K steps. Data are shown by circles with error bars, with the thin black lines showing the existence of a T_g feature. The thick black line denotes experimental data from ref 11, with dashed extensions being extrapolations from these data.

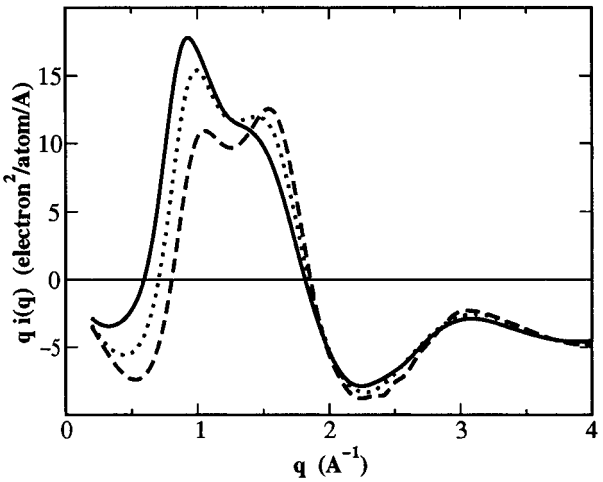

Figure 2. *s*-weighted reduced intensity function obtained from WAXS measurements at 500 K (—), 400 K (· · ·) and 300 K (– – –).

For one cell this reduction was in steps of 25 K, running MD for 100 ps at each temperature (to allow an observation of the computer glass transition temperature as discussed below). Configurations were saved at 100 K intervals, and a further 1 ns of MD run on these saved configurations. For the other four cells the temperature was reduced in 100 K steps, running MD for 1 ns at each step.

All MD runs used the NPT ensemble, with temperature control by the Anderson method and pressure by the Berendsen method (pressure decay constant 0.5 ps and compressibility 0.5). The pressure was set to 0, which is indistinguishable from 1 atm. The Discover package from MSI was used with the Polymer Consortium Force Field II (PCFF2), 8.5 Å group based cutoffs and a tail correction applied to the nonbond energy and pressure because of the cutoff.[10] The time step used was 1 fs. The permittivity was set to 1. The effect of variation of the permittivity was not investigated since the cells produced showed excellent agreement with experimental density data, and the motion of the nonpolar methyl groups is expected to be dominated by density effects.

From the last 600 ps of each 1 ns runs, all the atom coordinates were recorded at 5 ps intervals and the dihedral angles of all rotatable bonds recorded at 0.1 ps intervals.

Computer Glass Transition. The temperature dependence of the volume measured during the cooling run for the first cell is shown in Figure 1. When the temperature is changed, it takes a number of MD steps before the energy of the system reaches an equilibrium. The volume was therefore obtained by averaging over the second half of the MD simulation at each temperature, after equilibration had been achieved.

The results show a glass transition (T_g) like feature at 325 K. Above this temperature the simulation results are in good agreement with experimental data;[11] however, the experimental T_g is much lower at 250 K.

We term the simulation T_g as a "computer glass transition". The limits to the length of MD possible lead to a very high cooling rate (2.5×10^{11} K s^{-1}) and thus a high T_g. While it is not a very good estimate of the experimental T_g, it is of relevance to simulation in that it shows that the system is likely to be conformationally equilibrated above this temperature, while below it equilibrium will not be obtained and the structures will be essentially those obtained on cooling through the computer T_g.

Validation of Simulation Cells. To validate the short-range structures obtained in the simulation cells, experimental wide-angle X-ray scattering (WAXS) data were obtained for a sample of PVME supplied by Scientific Polymer Products Co. These experiments were performed at the Polymer Science Centre, University of Reading, using procedures developed there.[12] *q*-weighted reduced intensity function measurements were obtained from the WAXS data at 25 K intervals between 300 and 500 K. For clarity Figure 2 shows the results at just three temperatures.

To calculate the corresponding data from the simulation, the atom positions recorded at 5 ps intervals during the MD runs at each temperature were used. The following formula[13] was used, averaging over each of the frames in the simulation.

$$i(q) = \langle\rho\rangle \int \mathrm{d}r\, 4\pi r^2 \frac{\sin qr}{qr} \sum_i^n \sum_j^n x_i x_j f_i(q)\, f_j(q)[g_{ij}(r) - 1] \quad (1)$$

where $\langle\rho\rangle$ is the average number density of all atoms in the system, x_i and x_j are fractional compositions of the different atom species, and $f_i(q)$ and $f_j(q)$ are structure factors. The sums are over the n different atom species. $g_{ij}(r)$ is the pair distribution function, defined as $\rho_{ij}(r)/\langle\rho_j\rangle$ where $\rho_{ij}(r)$ is the density of atom species j at a distance r from an atom i.

The results for one simulation cell are shown in Figure 3 for the same three temperatures as shown for the experimental data. The features of the pattern are similar to the experimental data, although the position of the peak around 1 Å^{-1} is higher in the simulated data. We may thus conclude that our simulation cells have a reasonable structure.

In both cases the higher q peaks at around 5.5 Å^{-1} (not shown) and 3 Å^{-1} are temperature-independent. These arise from directly bonded atoms (at about 5.5 Å^{-1}) and from two atoms bonded to a common third atom (at about 3 Å^{-1}). The low-q peaks are temperature-dependent. The 1 Å^{-1} peak shifts to higher q as the temperature decreases. While it might reasonably be

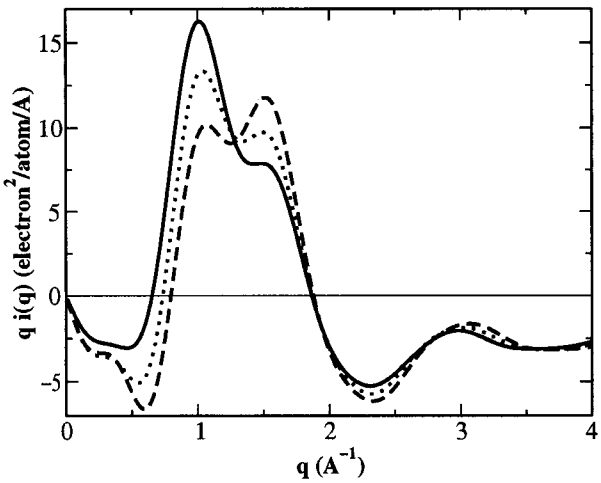

Figure 3. Calculated *s*-weighted reduced intensity function at 500 K (—), 400 K (· · ·), and 300 K (– – –).

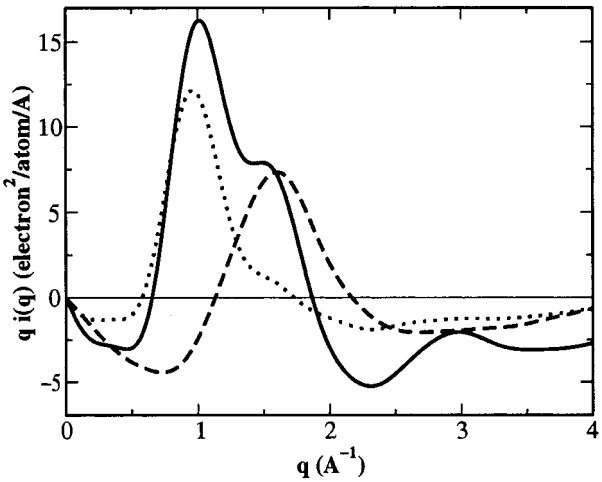

Figure 4. Calculated *s*-weighted reduced intensity function at 500 K calculated either from the backbone atoms only (· · ·) or from the side group atoms only (– – –), compared with that from all atoms (—).

surmised that this peak relates to the distance between polymer chains, the 1.6 $Å^{-1}$ peak is harder to assign.

It is interesting to process the simulated reduced scattering intensities in order to investigate the origin of these low-*q* peaks. An intensity function can be calculated by considering either only the atoms in the polymer backbone or only the atoms in the side groups. The results are shown in Figure 4 (where it should be noted that the sum of the two partial intensity plots will not sum to the total pattern since cross terms between backbone and side group atoms are excluded from both partial sums). These results show that the 1 $Å^{-1}$ peak originates from the backbone atoms while the 1.6 $Å^{-1}$ peak originates from the side group atoms. As the temperature is reduced, it might be expected that there will be an increasing proportion of low-energy backbone conformations which will allow for a more regular placement of side groups and thus an increase in the intensity of this latter peak.

Whole Cell Dynamic Analysis

For each temperature and for each cell analyzed the position of each methyl group was recorded at 0.1 ps intervals during the final 600 ps of the MD simulations. An excerpt of the record for a typical group at 200 K is shown in Figure 5. Here it can be seen that the dihedral can be considered to be in one of three states with angles librating about 0° or ±120°, with transitions between the states. A transition is counted when the dihedral angle crosses the values dividing the three states at 180° or ±60° (indicated by horizontal lines in the figure). The rate of transition between states is clearly much lower than the sampling frequency, and the possibility that a methyl group makes more than one transition between two samples can be neglected.

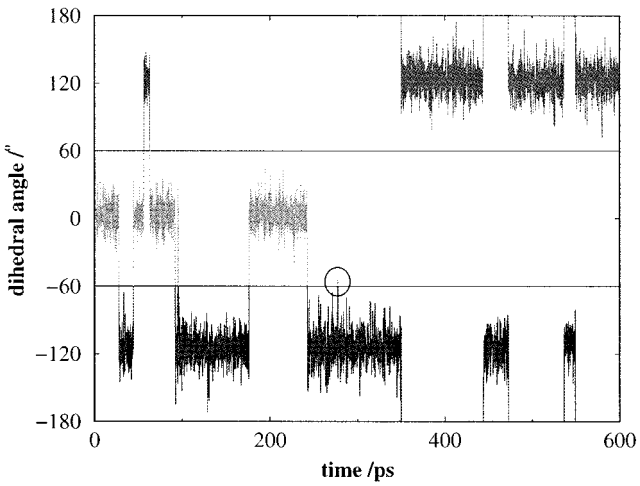

Figure 5. Dihedral angle as a function of time for a typical methyl group. The horizontal lines divide the angle into three "states". The circle indicates a possible source of miscounting of transitions as discussed in the text.

Table 1. Average Transition Rates (Transitions per Methyl Group per ps) Measured for All Five Cells

	500 K	400 K	300 K	200 K	*E* (kcal/mol)	τ_0 (fs)
mean	1.07	0.69	0.33	0.076	1.76	159
std dev	0.02	0.003	0.01	0.004	0.04	8

In the figure another possible cause of miscounting transitions is circled—because of its environment, this particular group appears to be librating about a slightly different value from −120°. A more detailed study would recalculate the state boundaries for each group (which might possibly change as the simulation proceeds). However, the observed cases of this occurring are small, and so this too is neglected at present.

Rate of Conformational Change. The simplest way of analyzing the methyl group dynamics is to count the number of state transitions occurring during a fixed simulation time at each temperature, and a mean transition rate, Γ, can be obtained. Although there are no experimental data that directly measure this transition rate, the data can be fitted to a standard Arrhenius function:

$$\Gamma = \Gamma_0 \exp\left(-\frac{E}{RT}\right) \qquad (2)$$

where $\Gamma_0 = 1/\tau_0$ is related to the attempt frequency, *R* is the gas constant, and *E* is the activation energy for the transition. Values for τ_0 and *E* are thus obtained, and the results are shown in Table 1. This simple approach may then be compared with the correlation function approaches described later.

Autocorrelation Function. For a more sophisticated analysis of this process, a conformational state function is defined $c(t_1,t_2)$ which equals unity if a dihedral is in the same state at times t_1 and t_2 and

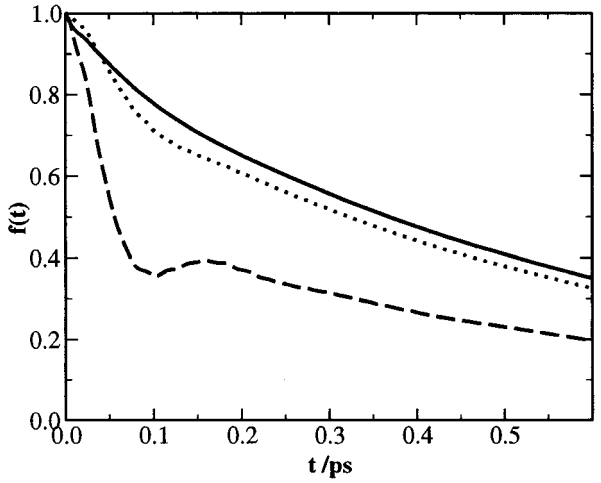

Figure 6. Comparison between the conformational state autocorrelation function (—) and the $P_1(\cos\theta)$ (· · ·) and $P_2(\cos\theta)$ (– – –) correlation functions.

equals 0 otherwise. Then a conformational state autocorrelation function is given by

$$f(t) = \langle c(t', t' + t)\rangle \tag{3}$$

where the angle brackets denote an average taken over all time origins t' and over all methyl groups. This process is similar to that used by Brown and Clarke[14] to describe conformational relaxations in butane and by us to describe the behavior of methyl groups in PMMA.[1] This can be normalized to vary from 1 to 0:

$$F(t) = \frac{f(t) - f(0)}{f(\infty) - f(0)} \tag{4}$$

This conformational state autocorrelation function only takes into account the transitions between the different states, not the motion within a state. This is in contrast to the more commonly used $P_1(\cos\theta)$ or $P_2(\cos\theta)$ correlation function, whose value will fall with t even if no state transitions occur (see Figure 6).

KWW Analysis of Correlation Function. The conformational state autocorrelation function can be fitted to the stretched exponential or KWW function:

$$f(t) = \exp\left(-\left(\frac{t}{\tau}\right)^{\beta}\right) \tag{5}$$

The relaxation time τ and stretching parameter β are to be fitted. $\beta = 1$ corresponds to a single relaxation time, while as β falls the range of relaxation times increases.

This function has been used previously to fit quasielastic neutron scattering data[2] and simulation results[1] for PMMA.

The results of the fit are shown in Table 2, where each set of data were fitted over the same range of correlation function $f(t)$ rather than the same range of time. The range chosen was until $f(t)$ had fallen to either 0.1 or 0.01. (These are indicated by the horizontal lines in Figure 7.) The data were weighted by the expected counting error in each point, which increases as $f(t)$ falls toward 0. Fitting was performed on data from each of the five cells; the standard deviation between these values was of the order of 1% of the calculated parameter values at 500 K, raising to 6% at 200 K. The standard deviation was similar for both ranges of fitting.

Table 2. Average Fitting Parameters for the KWW Fit to the Whole Cell State Autocorrelation Function

	fit to $f(t)>0.01$		fit to $f(t)>0.1$		std dev[a]	
temp (K)	τ (ps)	β	τ (ps)	β	τ (ps)	β
500	0.59	0.82	0.59	0.84	0.007	0.002
400	1.08	0.84	1.08	0.84	0.010	0.007
300	2.80	0.83	2.78	0.84	0.09	0.010
200	17.4	0.73	17.0	0.75	1.1	0.018

[a] Standard deviations of the values calculated for each of the five cells were similar regardless of the range of fitting.

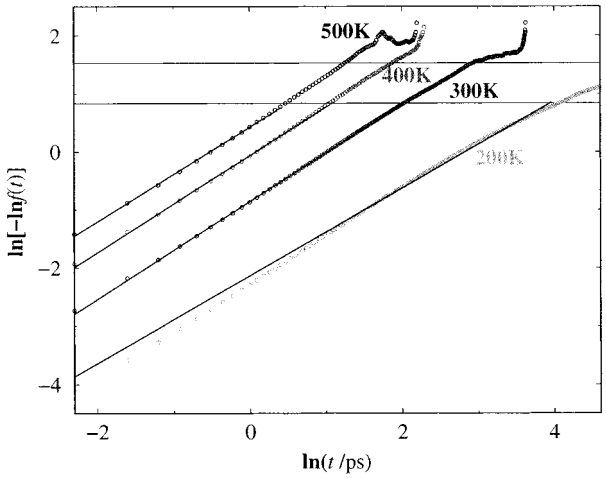

Figure 7. KWW fit to conformational state autocorrelation function at the temperatures indicated. Small circles are the data, and the sloping lines are the fits over the range $1 > f(t) > 0.1$. The horizontal lines indicate the alternate limit of the ranges of $f(t)$ over which the fitting was performed ($f(t) = 0.1$ corresponds to the lower line, and $f(t) = 0.01$ corresponds to the upper line).

Figure 7 shows the fitted KWW function compared with the autocorrelation data. Note that the fits were performed using directly the values of $f(t)$; they have been plotted logarithmically here in order to illustrate the expected straight line relationship from the form of the KWW function. Because of the logarithmic time axis there are many more points toward the right-hand side of the graphs. From these fits, values of τ and β were obtained at each temperature. At the lower temperatures the differences between the five simulation cells were greater, and in general the quality of the KWW fit became poorer.

By using the Arrhenius relationship, values of τ_0 and E were calculated from the temperature variation of τ. A good straight line was obtained; it is interesting to note that the "computer T_g" was not seen in this plot. The values obtained did not vary significantly with the range of $f(t)$ fitted, yielding values of 2.23 kcal mol^{-1} and 65 fs for E and τ_0, respectively.

RRDM Analysis of Correlation Function. A second method of analyzing the conformational state autocorrelation function is to use the rotational rate distribution model (RRDM).[4] This assumes that the methyl groups have a *distribution* of transition rates and hence that the conformation function can be fitted to

$$F(t) = \int e^{-t/\tau} g(\ln\tau)\, d(\ln\tau) \tag{6}$$

where g, the distribution of $\ln\tau$, is a Gaussian function. The fitting parameters are then the mean $(\ln\tau)_{mid}$ and standard deviation $\Delta_{\ln\tau}$ of this Gaussian distribution.

Table 3. Average Parameters from RRDM Fitting to Whole Cell State Autocorrelation Function

	fit to $f(t)>0.01$			fit to $f(t)>0.1$			std dev[a]	
temp (K)	τ_{mid} (ps)	$\Delta_{ln\tau}$	Δ_E (kcal/mol)	τ_{mid} (ps)	$\Delta_{ln\tau}$	Δ_E (kcal/mol)	τ_{mid} (ps)	$\Delta_{ln\tau}$
500	0.56	0.62	0.62	0.57	0.75	0.75	0.006	0.005
400	1.03	0.59	0.47	1.04	0.70	0.56	0.009	0.02
300	2.65	0.63	0.38	2.65	0.69	0.41	0.09	0.03
200	15.5	0.95	0.38	15.5	0.94	0.38	1.0	0.05

[a] Standard deviations of the values calculated between each of the five cells were similar regardless of the range of fitting.

Results are shown in Table 3. The results for $\Delta_{ln\tau}$ are somewhat more sensitive to the range of data fitted. The variation of results between the five simulation cells was of a similar order of magnitude as observed previously with the KWW fits.

If we write

$$\tau = \tau_0 \exp\left(\frac{E}{RT}\right) \tag{7}$$

then the relationship between $\Delta_{ln\tau}$ calculated and Δ_E, the spread of activation energies, is given by

$$\Delta_{\ln \tau} = \Delta_{\ln \tau_0} + \frac{\Delta_E}{RT} \tag{8}$$

Assuming a constant τ_0 (i.e., $\Delta_{\ln \tau_0} = 0$), we can therefore calculate the spread of activation energies, Δ_E, and these values are included in Table 3. The table shows this spread reducing as the temperature falls which suggests that at the lower temperatures some motions become frozen, and we are not accessing all possible methyl group environments. This is further discussed later when the behavior of individual methyl groups is considered. Below the computer T_g (i.e., the 300 and 200 K data) the spread of activation energies, Δ_E, remains constant with temperature at 0.38 kcal mol^{-1}. The experimental data[4] taken over a similar temperature range of 175−300 K show a similar near constant value of 0.43 kcal mol^{-1}.

The mean activation energy can be obtained from an Arrhenius fit to the $(\ln \tau)_{mid}$ data at the different temperatures. The results again are not dependent on the range of data fitted and are consistent between the different cells. The values of 2.18 kcal mol^{-1} and 65 fs for E and τ_0, respectively, are similar to the KWW calculations.

Individual Methyl Group Analysis

The results presented above have been averaged over all the methyl groups in the simulation and can be compared directly with experimental measurements. An advantage of molecular modeling is that the behavior of *individual* methyl groups can be independently studied to further investigate the origin of the features seen.

It is thus possible to perform the same three analyses as used for the whole cells. One can investigate directly the rate of conformational change for each group. Alternatively, a conformational autocorrelation state function for each individual methyl group can be calculated by summing over only different time origins in eq 3. These can then be analyzed using the same methods of KWW or RRDM fits.

Rate of Conformational Change. The number of transitions made by each methyl group was counted and a histogram produced of the distribution of numbers of transitions, binned using equal intervals on a logarithmic axis (Figure 8) to allow a comparison to be made with the distribution of ln τ.

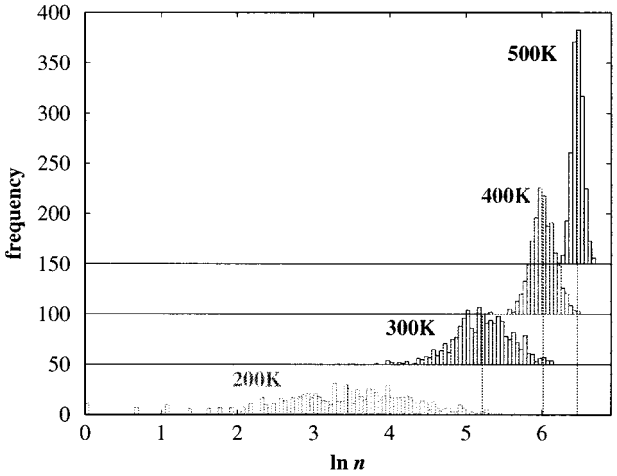

Figure 8. Distribution of numbers of transitions made by individual methyl groups at the temperatures indicated. For clarity plots are offset on the *y*-axis. The vertical lines indicate the means.

The Gaussian nature of these histograms adds credence to the choice of a Gaussian distribution in the RRDM fit.

The activation energy for the process and preexponential factor can be calculated in a similar manner as before, giving 2.01 kcal mol^{-1} and 119 fs for E and τ_0, respectively. These are quite different to the whole cell analysis. This difference arises because in the whole cell we average transition counts and then fit to a logarithmic expression, whereas in this analysis the fit is performed on each group, and then an average is taken; in one case we calculate $\ln\langle n\rangle$ and in the other $\langle \ln n\rangle$ where n is the counted number of transitions for each group.

Figure 9 illustrates the change in the mean value of ln Γ with temperature, from which the activation energy was calculated. Note that the "computer T_g" is not visible. (This was observed generally in all the Arrhenius plots made.) The standard deviation of the ln Γ are shown by the two dotted lines which correspond to $\ln \Gamma + \sigma_{\ln\Gamma}$ and $\ln \Gamma - \sigma_{\ln\Gamma}$ and appears to be collapsing to zero at a finite temperature. This implies a correlation between E and Γ_0 and has been referred to as a compensation law.[15] Such a correlation would invalidate the calculation of Δ_E from $\Delta_{ln\tau}$ as performed above.

A simple analysis of this correlation is to assume that the attempt frequency is related to the barrier height as follows. Assume that the energy of each methyl group as a function of angle is harmonic given by

$$E = \frac{E_b}{2}(1 - \cos 3\theta) \tag{9}$$

where E_b is the energy barrier. Considering small

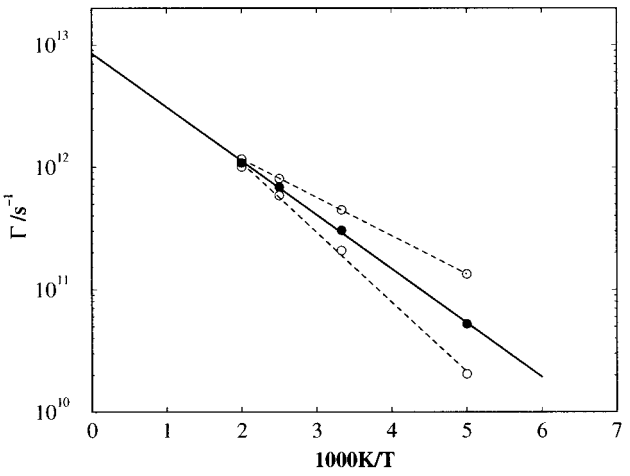

Figure 9. Temperature variation of the mean transition rate ln Γ (—) from which an activation energy can be calculated. The dashed lines represent ln $\Gamma \pm \sigma_{\ln\Gamma}$ and show the width of the distribution of transition rates observed in the transition rate analysis of individual groups.

fluctuations around the minimum energy position will give a restoring torque of

$$F = -\frac{dE}{d\theta} = -\frac{3}{2}E_b \sin 3\theta \approx -\frac{9}{2}E_b\theta = I\ddot{\theta} \quad (10)$$

and thus a harmonic frequency $\omega^2 \propto E_b$. The preexponential factor τ_0 will be proportional to $1/\omega$ and thus $\tau_0 \propto E_b^{-1/2}$ and

$$\Delta_{\ln \tau_0} = -\frac{1}{2}\Delta_{\ln E_b} = -\frac{1}{2}\frac{\Delta_{E_b}}{\bar{E}_b} \quad (11)$$

where $\bar{E}_b$ is the mean energy barrier. Substituting (11) into eq 8 gives

$$\Delta_{\ln \tau} = \Delta_{E_b}\left(\frac{1}{RT} - \frac{1}{2\bar{E}_b}\right) \quad (12)$$

which shows the behavior observed in Figure 9; i.e., $\Delta_{\ln\tau}$ is a function of temperature and falls to zero at a finite value of temperature. For a mean energy barrier of about 2 kcal mol^{-1} this temperature is 2000 K.

Evidence of such a correlation between τ_0 and E_b could be seen by studying the distribution of librational frequencies of the groups, and this work is underway at the present.

This analysis will hold at low temperatures where over the time of the simulation the environment of the group and hence the barrier height will be expected to change little (this is discussed further later). $\sigma_{\ln\Gamma}$ represents the range of difference in behaviors between groups averaged over the time of the simulation, and so at a high temperature this time averaging will be over a sufficient period that all the groups will have experienced the same averaged environment and so it would be expected that $\sigma_{\ln\Gamma}$ will tend to zero. At lower temperatures insufficient time will have been allowed for each group to experience the same time-averaged conformation. This will further contribute to the reduction in $\sigma_{\ln\Gamma}$ as the temperature increases.

KWW Analysis of Correlation Function. The conformational state autocorrelation function calculated for each individual methyl group may be calculated and then be fitted using the KWW function, obtaining values

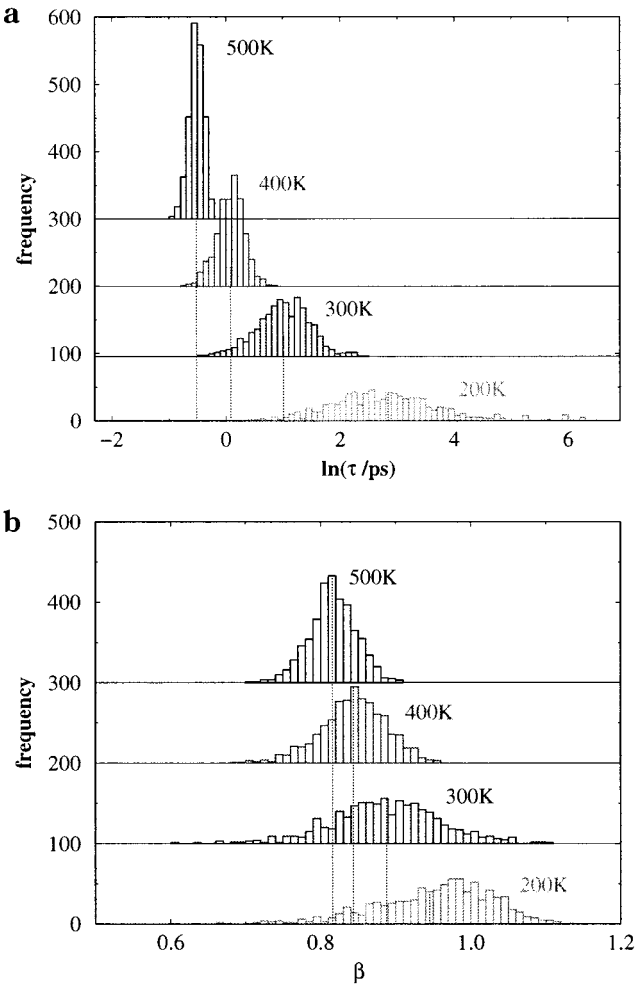

Figure 10. Plot of the results of applying the KWW fit to state autocorrelation functions calculated from each individual methyl group (a) ln τ and (b) β at the temperatures indicated. For clarity plots are offset on the y-axis. The vertical lines indicate the mean values.

of τ and β for each group. These are plotted in Figure 10 as histograms of the individual values of τ and β, where fitting has been performed over the range $1 > f(t) > 0.1$. Over the larger range $1 > f(t) > 0.01$ a similar pattern emerges, with broader distributions, particularly for β at the lower temperatures. At the lowest temperature some groups appear to have a nonrealistic value of $\beta > 1$; this is where the data are less accurate because of a small number of transitions. A scatter plot of τ and β values shows little correlation between τ and β at each temperature.

At high temperatures values of β show a narrow spread around $\beta = 0.8$. As the temperature is reduced, values tend toward 1 with a broader spread. A β of 1 would correspond to a single-exponential relationship and a hence a single relaxation time, while $\beta < 1$ corresponds to a range of relaxation times. So it appears that at high temperatures all the groups are behaving in a similar fashion, with a narrow range of τ values, while at lower temperatures individual methyl groups are more likely to exhibit a single relaxation time (as shown by $\beta \rightarrow 1$), but the different groups exhibit a wide range of relaxation times.

The values of τ tend from low values with a small spread at high temperatures toward higher values with a broader spread at low temperatures. An Arrhenius plot of the mean values of τ can be used to give a

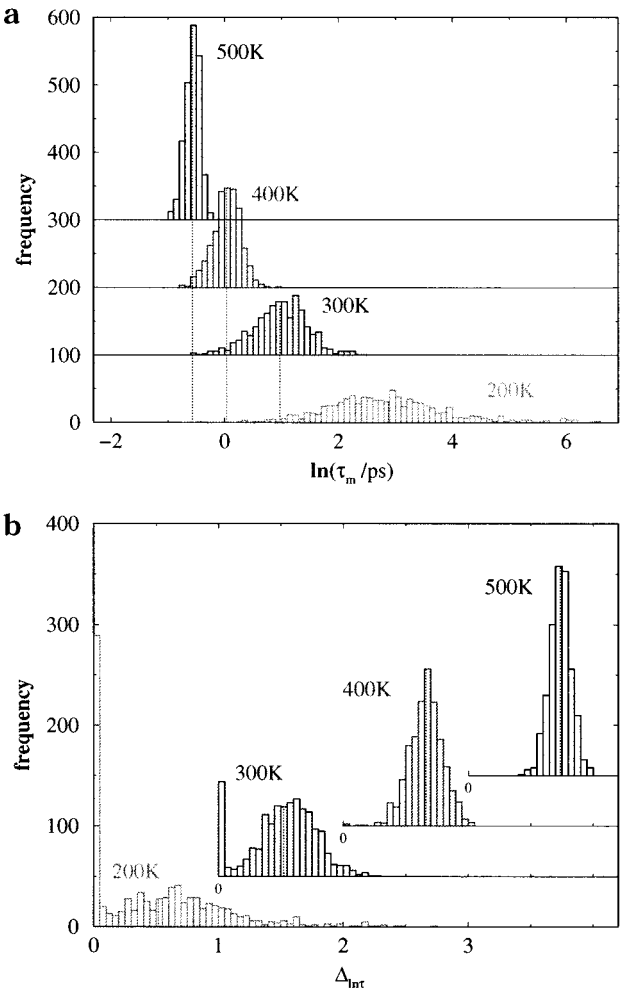

Figure 11. Plot of the results of applying the RRDM fit to state autocorrelation functions calculated from each individual methyl group. (a) ln τ_{mid} and (b) $\Delta_{ln\tau}$. Note that the plots in (a) have been shifted in the *y*-axis and those in (b) in both the *x* and *y* axes for clarity. The vertical lines indicate the mean values.

measure of the mean activation energy of the process of 2.23 kcal mol^{-1}. The increase in spread of τ as the temperature is reduced is to be expected from relation 8. The standard deviation calculated for the ln τ values plotted against temperature shows a similar behavior to that shown in Figure 9, again suggesting a correlation between E and τ_0. Since β changes over the temperature range considered, the mean values of τ could be corrected using the formula, obtained by integrating the KWW function:

$$\tau = \left(\frac{\tau_{KWW}}{\beta}\right)\Gamma(1/\beta) \qquad (13)$$

where Γ is the gamma function. An Arrhenius plot can then again be used to give another measure of the mean activation energy of the process of 2.45 kcal mol^{-1}.

RRDM Analysis of Correlation Function. Again the individual group conformational state autocorrelation function can be modeled using a RRDM fit, obtaining values for ln τ_{mid} and $\Delta_{ln\tau}$ for each group. These are illustrated as histograms in Figure 11 for the $1 > f(t) > 0.1$ fit. Again the fits over the larger range $1 > f(t) > 0.01$ are similar.

Similar behavior to that seen in the KWW analysis is again observed. A mean activation energy of 2.28 kcal mol^{-1} is obtained which is similar to previous values. As the temperature is reduced, the distribution of mean relaxation times (Figure 11a) increases, and a similar analysis to Figure 9 again shows evidence for a correlation between E and τ_0.

Figure 11b shows the distribution of relaxation times exhibited by individual methyl groups. As temperature reduces, the range of behaviors increases and a large number of methyl groups show a single-exponential behavior (as is seen by the large density of points collapsing to $\Delta_{ln\tau} = 0$). It is tempting to associate these groups with those in a "frozen" environment for the whole simulation period.

Summary of Barrier Height and Prefactor Values

All the results from the various analyses are shown in Table 4. We have excellent agreement for the mean activation energy between the correlation approaches and experiment, while the simple transition rate approach on the whole cell yields a significantly lower value. This can be understood by observing that the transition rate method will be biased toward those groups that make more transitions and therefore have a lower energy barrier. A single group making a large number of transitions can dominate the transition rate analysis but can only relax the correlation function a little. In contrast, the correlation function needs all groups to move in order to relax fully and is therefore more of an overall average. This bias has less of an effect when individual groups are considered.

The calculated result is very similar to the barrier to rotation calculated for an individual methyl group (2.1 kcal mol^{-1}), and so the primary effect of the environment is seen to broaden the distribution of activation energies rather than to increase the mean. Initially it may be expected that the environment will always increase the barrier to rotation, but a reduction of the barrier height can be brought about if the environment destabilizes the minimum energy position for a group.

The calculated values for the time constant τ_0 are also similar. The higher values calculated for the transition rate analysis are consistent with the correlation between E and τ_0 observed and discussed above.

Experimentally[4] the range of energy barriers ΔE is calculated using eq 8 giving a value of 0.43 kcal mol^{-1}, which is constant over the experimental temperature range 180−300 K. Our RRDM analysis also allows calculations to be made of this ΔE, assuming τ_0 is constant, and values of around 0.39 kcal mol^{-1} were obtained from the whole cell analysis over the same experimental temperature range (Table 3), which are in good agreement. However, the individual group analysis has suggested a correlation between E and τ_0, and so the calculation of ΔE in this manner is suspect.

Conclusions

Reasonable simulation cells can be obtained at high temperatures above the "computer T_g" at 325 K. At lower temperatures the structures may not be fully equilibrated.

Our simulation cells have been validated by calculating scattering patterns and comparing with experimental data. This shows two peaks at low q, with one at 1 Å^{-1} being associated with the backbone and one at 1.6 Å^{-1} being associated with the side groups. As the

Table 4. Activation Energies and Time Constants Calculated by the Various Methods Discussed[a]

	E (kcal/mol)				τ_0 (fs)			
	TR	KWW	RRDM	expt	TR	KWW	RRDM	expt
whole cell	1.76	2.33	2.18	2.0	159	64.4	65.1	83
		2.22	2.18			65.9	65.4	
individual groups	2.01	2.23 (2.47)	2.28		119	64.7	58.0	
		2.22 (2.50)	2.27			65.7	58.6	

[a] Where two numbers are given for the correlation fits then the first refers to data over the range $1 > f(t) > 0.01$ and the second to the range $1 > f(t) > 0.1$. The numbers in parentheses for the individual group KWW analysis refer to recalculation of the average τ as discussed in the text. The experimental data for comparison are from ref 4.

temperature is reduced, this latter peak increases in intensity, indicating some ordering of the side groups.

Molecular dynamics can be applied to simulate the state transitions in the methyl groups. The transition rate has been analyzed directly and through the fitting of a conformational state autocorrelation function with a KWW function or via the rotational rate distribution model. In all cases similar results were obtained for the activation energy of the process and for the time constant prefactor, with the RRDM fit being closer to experimental values.

The behavior of individual methyl groups could be studied. At high temperatures all methyl groups behave in a similar fashion, with each group exhibiting a nonexponential decay of the correlation function, while at low temperatures individual groups behave differently with a wide range of relaxation times, though each group tends to a single-exponential decay of the correlation function.

The wide range of relaxation times observed at the lower temperatures originates from the differing local environments for the groups. The presence of neighboring groups could affect the barrier energy either by reducing the energy of the transition state (where the local density is reduced) or by destabilizing and increasing the energy of the minimum. A future study might profitably consider an analysis of the local space available to the group, possibly by Voronoi polyhedra analysis.

Evidence is shown of a correlation between activation energy E and preexponential factor τ_0 from the reduction in spread of time constants observed with increasing temperature. Studies are in progress to investigate this further.

Acknowledgment. We thank Professor Mitchell for providing facilities for the X-ray characterization, Molecular Simulations Inc. for software, and the Thai Government for support for C. Saelee.

References and Notes

(1) Nicholson, T. M.; Davies, G. R. *Macromolecules* **1997**, *30*, 5501−5505.
(2) Arrighi, V.; Higgins, J. S. *Physica B* **1996**, *226*, 1−9.
(3) Williams, G.; Watts, D. C. *Trans. Faraday Soc.* **1970**, *66*, 80−85.
(4) Chahid, A.; Alegría, A.; Colmenero, J. *Macromolecules* **1994**, *27*, 3282−3288.
(5) Mukhopadhyay, R.; Alegría, A.; Colmenero, J. *Macromolecules* **1998**, *31*, 3985−3993.
(6) Colmenero, J.; Mukhopadhyay, R.; Alegría, A.; Frick, B. *Phys. Rev. Lett.* **1998**, *80*, 2350−2353.
(7) Molecular Simulations Inc., San Diego. Models built using Insight 400P and simulations performed by Discover 97.0.
(8) Theodorou, D. N.; Suter, U. W. *Macromolecules* **1985**, *18*, 1467−1478.
(9) Meirovitch, H. *J. Chem. Phys.* **1983**, *79*, 502−508.
(10) Huai, S.; Rigby, D. *Spectrochim. Acta A* **1997**, *53*, 1301−1323.
(11) Shiomi, T.; Hamada, F.; Nasako, T.; Yoneda, K.; Imai, K.; Nakajima, A. *Macromolecules* **1990**, *23*, 229−233.
(12) Mitchell, G. R. In *Comprehensive Polymer Science*; Allen, G., Bevington, J. C., Eds.; Pergamon Press: Oxford, 1989; Vol. 1, p 687.
(13) Mondello, M.; Yang, H. J.; Furuya, H.; Roe, R. J. *Macromolecules* **1994**, *27*, 3566−3574.
(14) Brown, D.; Clarke, J. H. R. *J. Chem. Phys.* **1990**, *92*, 3062−3072.
(15) Dufresne, A.; Lavergne, C.; Lacabanne, C. *Solid State Commun.* **1993**, *88*, 753−756.

MA991267P